Journal of Biomolecular NMR, **25:** 133–145, 2003.
KLUWER/ESCOM

Simultaneous measurement of protein one-bond and two-bond nitrogen-carbon coupling constants using an internally referenced quantitative *J*-correlated [^{15}N,^{1}H]-TROSY-HNC experiment

Hans L.J. Wienk[a], Mitcheell M. Martínez[a], Gary N. Yalloway[a], Jürgen M. Schmidt[b], Carlos Pérez[a], Heinz Rüterjans[a] & Frank Löhr[a,*]
[a]*Institut für Biophysikalische Chemie, J.W. Goethe-Universität, Marie-Curie-Str. 9, D-60439 Frankfurt am Main, Germany;* [b]*Research School of Biosciences, University of Kent at Canterbury, Canterbury, Kent CT2 7NJ, U.K.*

Received 16 September 2002; Accepted 27 November 2002

Key words: DFPase, flavodoxin, perdeuteration, residual dipolar coupling, scalar coupling, TROSY, xylanase

Abstract

A quantitative *J*-correlation pulse sequence is described that allows simultaneous determination of one-bond and two-bond nitrogen-carbon coupling constants for protonated or deuterated proteins. Coupling constants are calculated from volume ratios between cross peaks and reference axial peaks observed in a single 3D spectrum. Accurate backbone $^{1}J_{NC'}$, $^{1}J_{NC\alpha}$, and $^{2}J_{NC\alpha}$ coupling constants are obtained for the two [^{15}N;^{13}C]-labeled, medium-sized proteins flavodoxin and xylanase and for the [^{2}H;^{15}N;^{13}C]-labeled, large protein DFPase. A dependence of one-bond and two-bond $J_{NC\alpha}$ values on protein backbone ψ torsion angles is readily apparent, in agreement with previously found correlations. In addition, the experiment is performed on isotropic as well as aligned protein to measure associated ^{15}N-^{13}C residual dipolar couplings.

Abbreviations: C12E5 – *n*-dodecyl-penta(ethylene glycol); FMN – flavin-mononucleotide; R^2 – linear regression correlation coefficient; RDC – residual dipolar coupling; RMSD – root mean square deviation.

Introduction

One-bond and two-bond J_{NC} coupling constants carry valuable structure information. For instance, protein backbone-related $^{1}J_{NC'}$ couplings are sensitive to hydrogen bond formation, increasing and decreasing in value when hydrogen bonding involves peptidyl CO and NH sites, respectively (Juranić et al., 1995, 1996; Juranić and Macura 2001). $^{1}J_{NC\alpha}$ and $^{2}J_{NC\alpha}$ couplings were found to correlate with protein backbone torsion angles ϕ and ψ (Delaglio et al., 1991; Edison et al., 1994a, b; Wirmer and Schwalbe, 2002). Differences between ^{15}N-^{13}C couplings measured for isotropic and partially oriented protein molecules, also known as residual dipolar couplings (RDCs, D_{NC}), have been used as orientational restraints in structure calculations (Bax et al., 2001; De Alba and Tjandra, 2002).

Usually, one type of coupling is measured per NMR experiment, which might not always be a desired situation (De Alba et al., 2001). For example, when distinct RDCs are determined by different experiments for a partially oriented protein, the alignment of the protein sample may not be identical in each experiment. The complete equilibration of the alignment of the system may take days, and the orientation can also be influenced by varying heating effects during NMR pulsing in different experiments. Multiple coupling constants have been measured in a single spectrum (De Alba et al., 2001), using modified 3D HNCO (Kay et al., 1994) or (HA)CA(CO)NH (Tjandra and Bax, 1997) which simultaneously yield $^{1}J_{HN}$ and $^{1}J_{C'C\alpha}$ (or $^{1}J_{H\alpha C\alpha}$) from frequency differences using the IPAP strategy

*To whom correspondence should be addressed. E-mail: murph@bpc.uni-frankfurt.de

(Ottiger et al., 1998). Also, 3D HNCO(α/β-C′Cα-*J*)-TROSY and HNCO(α/β-NCα-*J*)-TROSY were reported to measure either the scalar couplings $^1J_{C'C\alpha}$ and $^3J_{HNC\alpha}$ or $^1J_{NC\alpha}$, $^2J_{NC\alpha}$, $^2J_{HNC\alpha}$, and $^3J_{HNC\alpha}$ concurrently (Permi et al., 2000). Furthermore, $^1J_{NC\alpha}$ and $^2J_{NC\alpha}$ coupling constants were measured concomitantly from $^{13}C^{\alpha}$ coupled, sensitivity enhanced [^{15}N,^{1}H]-HSQC spectra using either IPAP (Ottiger et al., 1998) or S^{3}CT techniques (Heikkinen et al., 2001), or employing an approach based on fitting peak intensities from sensitivity enhanced *J*-modulated [^{15}N,^{1}H]-HSQC spectra recorded with variable evolution periods (Wirmer and Schwalbe, 2002).

Alternative to frequency and *J*-modulation based methods, quantitative *J*-correlation experiments are used (Vuister and Bax, 1993a; Bax et al., 1994) in which the two nuclei of interest are correlated in an out-and-back manner with coupling constants then being encoded in intensity ratios between cross peaks and reference peaks. In the case of heteronuclear *J*-correlations cross-peak and reference-peak intensities are usually obtained from separate NMR spectra, possibly of different dimensionality (Vuister and Bax, 1993b; Vuister et al. 1993; Bax et al., 1994; Hu and Bax, 1997), making the evaluation of scalar coupling constants susceptible to experimental errors. Recently, a phase cycling scheme has been developed allowing to collect cross peaks and reference peaks in a single 3D spectrum (Löhr et al., 1999). In these experiments, magnetization is retained that has not been transferred between the two coupled nuclei, giving rise to axial peaks for internal reference. Here we describe a 3D quantitative *J*-correlated [^{15}N,^{1}H]-TROSY-HNC experiment for simultaneous observation of cross peaks and reference peaks for various types of one-bond and two-bond nitrogen-carbon couplings in a single 3D spectrum. Conceptually related to HNCO-type quantitative $J_{NC'}$ experiments (Cordier and Grzesiek, 1999; Cornilescu et al., 1999; Wang et al., 1999; Chou et al., 2000), the experiment utilizes simultaneous ^{15}N-^{13}C′ and ^{15}N-$^{13}C^{\alpha}$ magnetization transfer. In addition, a few simple alterations make the pulse sequence suitable also for deuterated proteins. For [^{15}N;^{13}C]-labeled xylanase and flavodoxin, and for [^{2}H;^{15}N;^{13}C]-labeled DFPase the reproducibility and accuracy of the quantitative *J*-correlated [^{15}N,^{1}H]-TROSY-HNC experiment is established. As a first application the correlation between protein backbone $J_{NC\alpha}$ coupling constants measured and ψ-angles is shown. Secondly, nitrogen-carbon residual dipolar couplings are measured for flavodoxin and tested for compatibility with its structure.

Description of the pulse sequence

The pulse sequence of the 3D quantitative *J*-correlated [^{15}N,^{1}H]-TROSY-HNC NMR experiment is depicted in Figure 1. The experiment is based on [^{15}N,^{1}H]-TROSY type (Pervushin et al., 1997) triple-resonance experiments such as HNCO and HNCA (Salzmann et al., 1998). Briefly, following the initial INEPT sequence, magnetization is transferred from ^{15}N to coupled ^{13}C spins. More specifically, for the protein backbone, magnetization is transferred from an amide ^{15}N to $^{13}C^{\alpha}$ of the current residue, and to both ^{13}C′ and $^{13}C^{\alpha}$ of the preceding amino acid. This is achieved in a HMQC manner (Bendall et al., 1983; Bax et al., 1983) upon which carbon magnetization is frequency labeled during t_1. To refocus $^{13}C^{\alpha}$-H^{α} couplings during evolution, a band selective 180° shaped pulse is applied to the α-protons, avoiding perturbation of $^1H^N$ spin states. After rephasing of ^{15}N antiphase magnetization with respect to carbons, nitrogen chemical shifts evolve during t_2 in a conventional rather than constant-time manner in order to minimize the number of refocusing pulses during the critical ^{15}N-^{13}C magnetization transfer steps and to allow for long ^{15}N acquisition times. Sensitivity enhanced echo-antiecho gradient selection of the relatively slowly relaxing ^{15}N and ^{1}H magnetization components is employed in the final TROSY steps (Czisch and Boelens, 1998; Pervushin et al., 1998; Dingley and Grzesiek, 1998; Weigelt, 1998; Loria et al., 1999). More experimental details are given in the legend to Figure 1.

Frequency labeling in t_1 separates magnetization components transferred from $^{15}N_i$ to either of the three coupled backbone ^{13}C-spins, giving rise to cross peaks at the $^{13}C^{\alpha}_i$, $^{13}C^{\alpha}_{i-1}$, and $^{13}C'_{i-1}$ frequencies in F_1. The signal intensities are modulated by the size of the respective active ^{15}N-^{13}C coupling constant, by two additional passive couplings, and by ^{15}N transverse relaxation. For example, the magnetization transfer giving rise to a cross peak at the ^{13}C carbonyl resonance position is proportional to

$$\begin{aligned}&A \cdot \sin[(\Delta + \tau_p/2)\pi^1 J_{NC'}] \cdot \sin[(\Delta - \tau_p/2)\pi^1 J_{NC'}]\\ &\cdot \cos[(\Delta + \tau_p/2)\pi^1 J_{NC\alpha}] \cdot \cos[(\Delta - \tau_p/2)\pi^1 J_{NC\alpha}]\\ &\cdot \cos[(\Delta + \tau_p/2)\pi^1 J_{NC\alpha}] \cdot \cos[(\Delta - \tau_p/2)\pi^1 J_{NC\alpha}]\\ &\cdot \exp(-2\Delta/T_{2(^{15}N)}),\end{aligned}$$

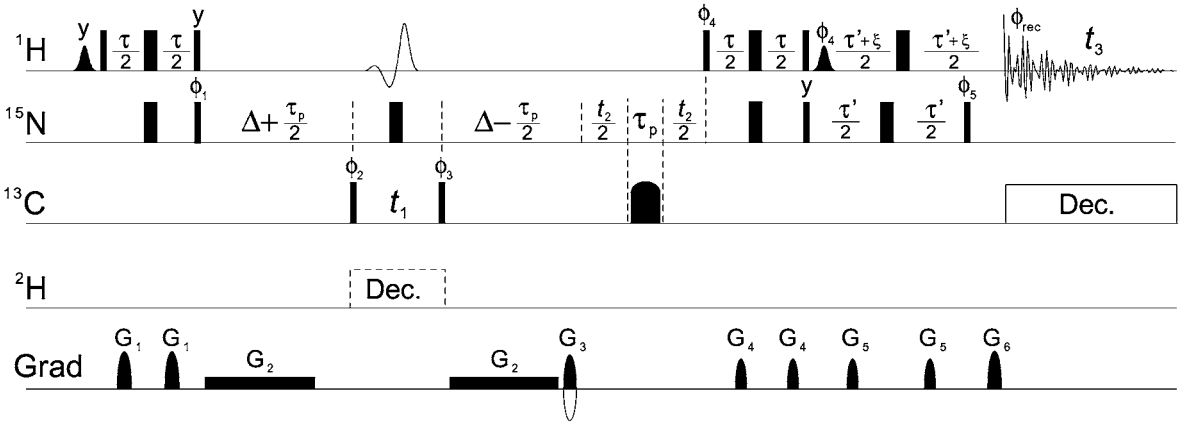

Figure 1. Pulse scheme of the 3D quantitative *J*-correlated [^{15}N,^{1}H]-TROSY-HNC experiment. Narrow and wide filled bars denote rectangular 90° and 180° pulses, respectively. RF field strengths applied are 20.8 kHz, 7.8 kHz and 25 kHz to ^{1}H, ^{15}N and ^{13}C, respectively. Carrier positions are 4.75 ppm (^{1}H), 118 ppm (^{15}N, centre of amide region) and 117 ppm (^{13}C, midpoint between α-carbon and carbonyl region). Selective water-flip-back pulses have a Gaussian shape, truncated at 10%, and have a duration of 2.1 ms. The first 90° Gaussian shaped pulse in the proton channel aligns the water ^{1}H magnetization along the positive z-axis to avoid saturation of fast exchanging amide protons by pulsed field gradients (Grzesiek and Bax, 1993; Stonehouse et al., 1994; Matsuo et al., 1996). Heteronuclear decoupling during acquisition is implemented as a sequence of 3-ms WURST-20 (Kupče and Freeman, 1995) pulses (60 kHz sweep) in a five-step supercycle (Tycko et al., 1985). The shaped 180° ^{13}C pulse for the refocussing of ^{15}N-^{13}C couplings during t_2 is a WURST-20 pulse (80 kHz sweep) with a duration τ_p of 0.5 ms. $^{13}C^{\alpha}$-$^{1}H^{\alpha}$ splittings are eliminated by the application of a 1.25-ms I-SNOB-3 (Kupče et al., 1995) pulse on α-protons in the centre of t_1, thus avoiding the interchange of amide proton spin states. In order to use the experiment for [^{2}H;^{15}N;^{13}C]-labeled proteins, the latter pulse is omitted, the phase of the initial water-selective 90° pulse is inverted and WALTZ-16 ^{2}H decoupling is applied with an RF field of 0.9 kHz. Delay durations are: $\tau = 4.6$ ms, $\Delta = 10$ ms, $\tau' = 5.4$ ms, $\xi = 0.4$ ms. The initial t_1 is set to half the increment step size such that the flanking ^{13}C pulses overlap with the $^{1}H^{\alpha}$-selective pulse for $t_1 < \tau_{(180°\,^{1}H^{\alpha})}$. Quadrature detection in the carbon dimension is accomplished by altering ϕ_2 in the States manner (States et al., 1982). Phase cycles are $\phi_1 = 2(x), 2(-x)$; $\phi_2 = x$; $\phi_3 = x$; $\phi_4 = y$; $\phi_5 = x$; $\phi_{rec} = 2(x), 2(-x)$ for the real part and $\phi_1 = 2(x), 2(-x)$; $\phi_2 = y$; $\phi_3 = x, -x$; $\phi_4 = y$; $\phi_5 = x$; $\phi_{rec} = x, 2(-x), x$ for the imaginary part of each t_1 increment. Pulse phases are x unless stated otherwise. G_2 is a rectangular z-gradient applied with an amplitude of 1 G/cm to prevent radiation damping during the Δ delays. All other z-gradients are sine-bell shaped and have the following lengths and peak amplitudes G_1: 0.5 ms, 5 G/cm; G_3: 1.6 ms, 39.45 G/cm; G_4: 0.3 ms, 4 G/cm; G_5: 0.3 ms, 5.5 G/cm; G_6: 0.2 ms, 32 G/cm. Echo- and antiecho coherence transfer pathways are acquired alternately by inversion of G_3 and the pulse phases ϕ_4 and ϕ_5. The two transients are stored separately and then added and subtracted to form the real and imaginary parts of a complex interferogram with a 90° zero-order phase shift added to one of the components.

where A is an amplitude factor depending on experimental conditions such as the number of scans and protein concentration (Chou et al., 2000), Δ is the coupling evolution delay, τ_p is the length of the refocusing 180° ^{13}C pulse, and $T_{2(^{15}N)}$ is the transverse relaxation time of the coupled nitrogen. Because $\tau_p \ll \Delta$ and $\tau_p \ll 1/J$, this expression is approximated by

$$A \cdot \sin^2(\Delta\pi^1 J_{NC'}) \cdot \cos^2(\Delta\pi^1 J_{NC\alpha}) \cdot \cos^2(\Delta\pi^1 J_{NC\alpha}) \cdot \exp(-2\Delta/T_{2(15N)}). \quad (1)$$

The delay Δ is chosen such that cross-peak attenuation due to passive nitrogen-carbon coupling interactions is minimized.

For each complex t_1 increment, two FIDs are recorded according to the States protocol (States et al., 1982) using different phases cycles for the real ($\phi_2 =$ x) and imaginary part ($\phi_2 =$ y), as described previously (Löhr et al., 1999, 2000; Löhr and Rüterjans, 2001). In the real part, the phase of the second 90° pulse on carbons (ϕ_3) is not phase cycled, retaining magnetization that is not transferred via ^{15}N-^{13}C coupling, whereas phase cycling in the imaginary part rejects this magnetization. The fraction of magnetization retained constitutes the reference intensity proportional to

$$A \cdot \cos^2(\Delta\pi^1 J_{NC'}) \cdot \cos^2(\Delta\pi^1 J_{NC\alpha}) \cdot \cos^2(\Delta\pi^2 J_{NC\alpha}) \cdot \exp(-2\Delta/T_{2(^{15}N)}), \quad (2)$$

giving rise to axial signals that are not modulated by ^{13}C chemical shift, which makes them appear in the plane $F_1 = 0$. As cross-peaks and reference peaks form part of the same dataset, the amplitude factors in Equations 1 and 2 are identical. Generally, such *J*-correlated experiments encode the coupling constant in the ratio between cross-peak and reference-peak intensity (Bax et al., 1994), according to

$$V_{cross}/V_{ref} = \tan^2(\Delta\pi J), \quad (3)$$

where J stands for $^{1}J_{NC'}$, $^{1}J_{NC\alpha}$ or $^{2}J_{NC\alpha}$ in the present application. Since all carbon chemical shifts

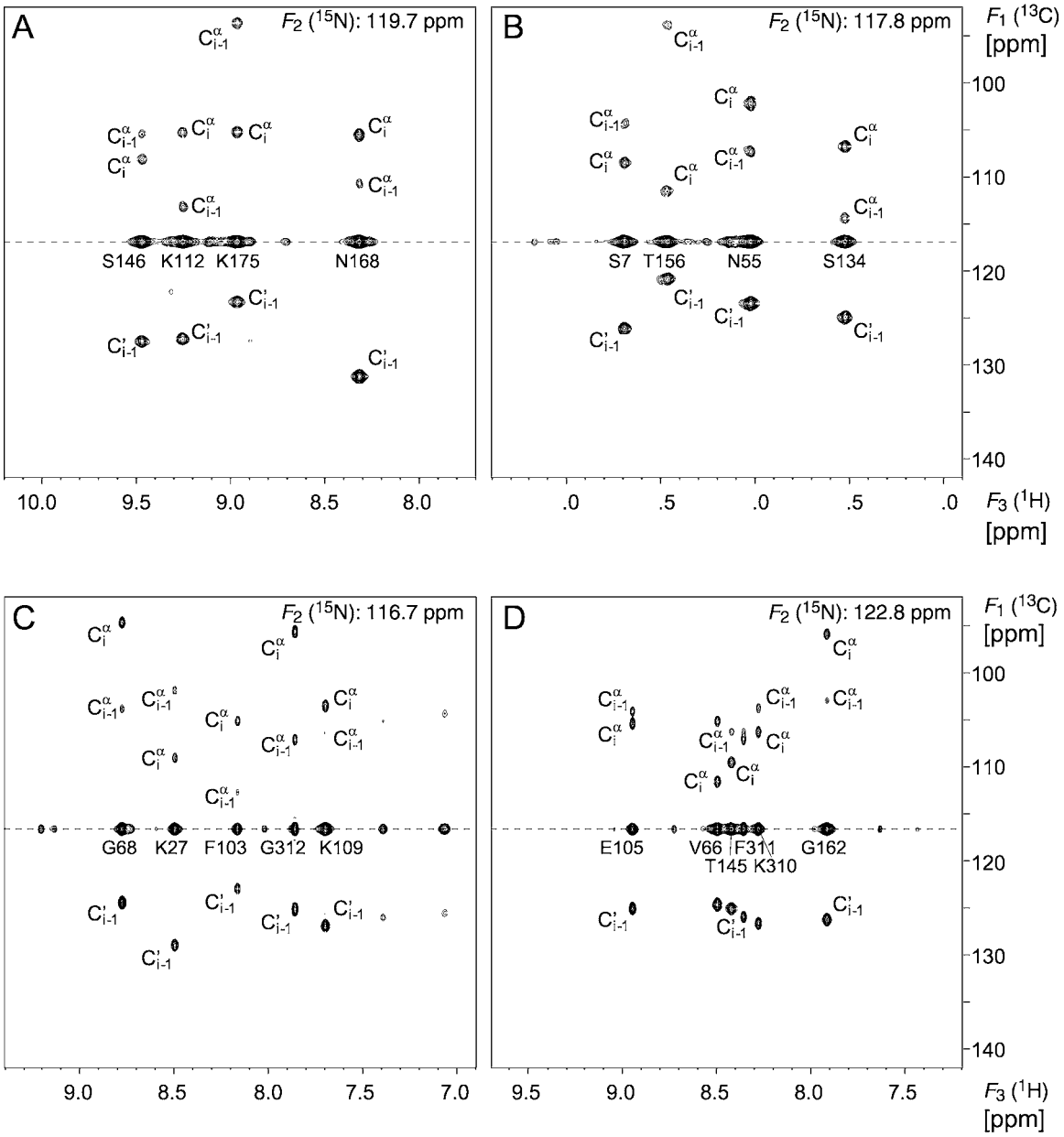

Figure 2. Selected $^{1}H^{N}$-^{13}C regions of 3D quantitative *J*-correlated [^{15}N,^{1}H]-TROSY-HNC spectra recorded for (A, B) [^{15}N;^{13}C]-xylanase, and (C, D) [^{2}H;^{15}N;^{13}C]-DFPase. The ^{15}N frequency is indicated in each region, dashed lines visualize the ^{13}C carrier frequency and the amino acid assignment is shown under the respective reference peak. Cross peaks are labeled C'_{i-1}, C^{α}_{i} and C^{α}_{i-1} and are aliased once. Unlabeled signals are spurious tails from peaks of significant intensity in adjacent planes.

evolve simultaneously during t_1 the $^{13}C'$ and $^{13}C^{\alpha}$ mutual scalar coupling cannot be refocused, causing lines to be broader for the cross peaks than for reference peaks, necessitating the use of peak volumes rather than peak intensities for analysis.

Materials and methods

NMR samples and general measurement conditions

Doubly labeled Family-11 [^{15}N;^{13}C]-xylanase from *Bacillus agaradhaerens* was purified after overexpression in *Escherichia coli*, essentially as described

(Sabini et al., 1999). The NMR sample contained 1.5 mM xylanase, 10 mM Na-d_3-acetate at pH 5.3, and 5% (v/v) D_2O. Triply labeled [^{2}H;^{15}N;^{13}C]-DFPase from *Loligo vulgaris* was purified after overexpression in *E. coli* (Hartleib and Rüterjans, 2001). The NMR sample contained 0.75 mM DFPase, 10 mM 1,3-bis[tris(hydroxymethyl)methylamino]propane (Bis-Tris propane) at pH 6.5, 5 mM $CaCl_2$, and 5% D_2O. Doubly labeled [^{15}N;^{13}C]-flavodoxin from *Desulfovibrio vulgaris* was expressed and purified from *E. coli* (Curley et al., 1991; Knauf et al., 1993). The NMR sample contained 2.1 mM flavodoxin in 20 mM KP_i at pH 7.0, 0.3 mM EDTA, and 5% (v/v) D_2O. Flavodoxin was aligned in the magnetic field by addition of C12E5 / hexanol in a molar ratio of 0.8 (Rückert and Otting, 2000) from a five-fold concentrated stock solution in the same buffer as the isotropic sample. Final protein and C12E5 concentrations were 1.5 mM and 5% (w/v), respectively. Each NMR sample also contained 0.15 mM 3-(trimethylsilyl)-1-propanesulfonic acid (DSS) as internal standard, 50 μg/ml Pefabloc protease inhibitor, and 0.03% (w/v) sodium azide.

All NMR experiments were recorded at 800 MHz on a Bruker Avance spectrometer equipped with a 5 mm ^{1}H{^{15}N,^{13}C} z-gradient triple resonance probe. Each experiment was performed twice and spectra were processed with Bruker XWIN-NMR software. NMR experiments on xylanase and DFPase were carried out at 301 K. Isotropic and aligned flavodoxin were measured at 299 and 296 K, respectively. Single-scan ^{2}H-NMR experiments were performed to monitor the orientation of the system used for flavodoxin alignment.

Quantitative J*-correlated [^{15}N,^{1}H]-TROSY-HNC experiments*

Acquisition parameters used to measure different protein samples with 3D quantitative *J*-correlated [^{15}N,^{1}H]-TROSY-HNC experiments are given in the legend to Figure 1 and in Table 1. To assess their precision each experiment was performed twice. For xylanase and flavodoxin samples different ^{13}C carrier frequencies were employed in the two experiments to account for accidental overlap of cross peaks and reference peaks. This yielded extra coupling constants for two and nine residues, respectively. Two and four scans per FID were recorded for isotropic flavodoxin and all other samples, respectively. Prior to zero-filling and Fourier transformation, time domain data were extended by approximately 50% using linear prediction in both indirect dimensions, followed by squared-cosine apodization in all three dimensions. Cross-peak and reference-peak volumes were determined using Matlab routines.

All ^{13}C′ and ^{13}C$^\alpha$ resonances were folded once in the F_1 dimension. Depending on the RF field strength of the ^{13}C 90° pulses applied, the cross-peak volumes in quantitative *J*-correlation experiments are affected by off-resonance effects, which can be corrected for either by calculation (e.g., Konrat et al., 1997) or experimentally. To assess the influence of the field strength applied at 25 kHz experimentally, the quantitative *J*-correlated [^{15}N,^{1}H]-TROSY-HNC was applied in a two-dimensional [^{13}C,^{1}H]-version omitting the t_2 period including the ^{13}C inversion pulse τ_p, with prolonged Δ periods (24 ms), each containing a ^{13}C$^\alpha$-selective refocusing pulse in its midpoint, such that only ^{15}N-^{13}C′ magnetization transfer takes place. The experiment was performed twice with [^{2}H;^{15}N;^{13}C]-labeled DFPase, switching the position of the ^{13}C carrier frequency between the center of the carbonyl region (on-resonance at approx. 175 ppm) and the usual average of ^{13}C′ and ^{13}C$^\alpha$ region (off-resonance at approx. 117 ppm). The 48 well-resolved cross-peaks that were quantified revealed almost negligible variations in peak intensities at the RF field employed throughout this study (a factor of 0.99 ± 0.02 was found). Nevertheless, cross-peak volumes were corrected before evaluating *J* according to equation 3.

Control NMR experiments

Spin-state selective 2D HN(α/β-NC′-*J*)-TROSY and 2D HN(CO-α/β-NCα-*J*)-TROSY (Permi and Annila, 2000) were recorded to collect control values for $^1J_{NC'}$, $^1J_{NC\alpha}$, and $^2J_{NC\alpha}$. Acquisition parameters are made available as supplementary material. Spectra were processed using squared sine-bell window functions, shifted by π/2 in F_2 and π/3 in F_1, and zero-filling. The digital resolution in F_1, where splittings due to nitrogen-carbon couplings arise, was in the range from 1.2 to 1.6 Hz/pt. The frequency differences between the multiplet lines forming the control coupling constants were determined using Matlab routines performing a 2D multiplet fit.

Table 1. Acquisition parameters used for measuring protein $^1J_{NC'}$, $^1J_{NC\alpha}$ and $^2J_{NC\alpha}$ couplings by 3D quantitative *J*-correlated [^{15}N,^{1}H]-TROSY-HNC

Protein sample	Exp.	Time domain points[a]		Acquisition times (ms)		Spectral widths (ppm)		^{13}C carrier	Measurement time
		t_2 (^{15}N)	t_3 (^{1}H)	t_2 (^{15}N)	t_3 (^{1}H)	F_2 (^{15}N)	F_3 (^{1}H)	(ppm)	(h)
Xylanase	1	216	768	100.2	73.2	26.6	13.1	118.0	57
	2	152	768	124.9	73.2	15.0	13.1	117.0	47
DFPase	1	152	896	125.2	91.8	15.0	12.2	116.7	63
	2	152	896	138.8	91.8	14.0	12.2	116.7	64
Flavodoxin (isotropic)	1	216	768	133.2	81.2	20.0	11.8	118.6	34
	2	192	768	148.0	81.2	16.0	11.8	116.6	30
Flavodoxin (aligned)	1	148	640	91.2	67.7	20.0	11.8	118.7	42
	2	134	640	103.3	67.7	16.0	11.8	116.7	38

[a]Number of complex points. For t_1 (^{13}C), the number of complex points and acquisition time were 52, and 5.2 ms, respectively, and the F_1(^{13}C) spectral width was 50 ppm in all experiments.

Results and discussion

Quantitative J*-correlated [^{15}N,^{1}H]-TROSY-HNC experiment*

For larger proteins, perdeuteration is advantageous to reduce ^{13}C linewidths and, especially when combined with TROSY, also amide proton and nitrogen linewidths. The proposed quantitative *J*-correlated [^{15}N,^{1}H]-TROSY-HNC experiment can be used for protonated as well as for deuterated proteins with minor changes to the pulse sequence. The functionality of the quantitative *J*-type experiment was tested with the [^{15}N;^{13}C]-labeled proteins flavodoxin (16 kDa) and xylanase (23 kDa), and with [^{2}H;^{15}N;^{13}C]-labeled DFPase (35 kDa). Excerpts of relevant spectrum regions are shown in Figures 2 and 3. In general, four peaks are detected in the carbon dimension for each backbone amide ^{15}N-^{1}H^N pair, namely the reference peak at the ^{13}C carrier frequency, and three cross peaks due to $^1J_{NC'}$ $^1J_{NC\alpha}$, and $^2J_{NC\alpha}$ coupling. Using a spectral width of only 50 ppm, ^{13}C′ resonances are folded into the low-field half of the F_1 dimension, while the majority of the ^{13}C$^\alpha$ cross peaks appear in the high-field half.

Unresolved passive splittings of both ^{13}C$^\alpha$ and ^{13}C′ resonances due to $^1J_{C'C\alpha}$ and of ^{13}C$^\alpha$ resonances due to $^1J_{C\alpha C\beta}$ result in a height attenuation of the cross peaks whereas reference peaks lack passive splittings. In addition, cross peaks are broadened relative to reference peaks due to transverse ^{13}C relaxation during t_1. These effects necessitate data evaluation from volume integrals to avoid systematic underestimation of the J_{NC} couplings constants derived. To minimize overlap of reference peaks, which are all located in a single plane of the 3D spectrum, high resolution is required in both proton and nitrogen dimensions. TROSY-type line narrowing (Pervushin et al., 1997) at high magnetic fields is therefore essential for the quantitative HNC correlation experiment.

Nitrogen-carbon coupling constants were calculated from peak volumes according to Equation 3. Resulting $^1J_{NC'}$ coupling constants lie between 12.3 and 17.5 Hz, $^1J_{NC\alpha}$ couplings range from 8.3 to 14.3 Hz, and values of $^2J_{NC\alpha}$ are found between 4.6 and 10.4 Hz. Due to accidental overlap of ^{13}C$^\alpha$ and $^{13}C^{\alpha}_{i-1}$ cross peaks fewer $^1J_{NC\alpha}$ and $^2J_{NC\alpha}$ values were obtained than for $^1J_{NC'}$. For each protein sample, the experiment was performed twice, and the combined results are summarized in Table 2. Due to very slow deuterium-proton back-exchange after protein expression in deuterated media, only approximately 200 out of 294 non-proline residues gave detectable ^{1}H^N signals in spectra of deuterated DFPase. Nevertheless, quantitative *J*-correlated [^{15}N,^{1}H]-TROSY-HNC yielded a total of 520 nitrogen-carbon coupling constants for DFPase, corresponding to 88.4% of all potentially measurable values. For xylanase, a total of 501 (83.9%) coupling constants were obtained and quantitative *J*-correlation experiments on unoriented and aligned flavodoxin gave 351 (81.3%) and 348 (80.6%) backbone coupling values, respectively (Table 2).

To assess the reproducibility of the 3D quantitative *J*-correlated [^{15}N,^{1}H]-TROSY-HNC experiments, pairwise root mean square deviations (RMSDs) in J_{NC} of 0.31, 0.24, 0.17, and 0.20 Hz were calculated for the four samples. Uncertainties appear to increase from $^1J_{NC'}$ to $^1J_{NC\alpha}$ to $^2J_{NC\alpha}$, inversely correlated with

Table 2. Summary of measured protein backbone nitrogen-carbon coupling constants in various proteins[a]

Protein	Coupling	Quantitative *J*-corr. exp.		Spin-state selective methods	
		Number	RMSD (Hz)	Number	RMSD (Hz)
Xylanase	$^1J_{NC'}$	189	0.20	191	0.16
	$^1J_{NC\alpha}$	156	0.33	188	0.30
	$^2J_{NC\alpha}$	156	0.39	188	0.27
	Total	501		567	
DFPase	$^1J_{NC'}$	188	0.18	165	0.11
	$^1J_{NC\alpha}$	168	0.24	159	0.16
	$^2J_{NC\alpha}$	164	0.28	159	0.22
	Total	520		483	
Flavodoxin	$^1J_{NC'}$	128	0.11	128	0.06
(isotropic)	$^1J_{NC\alpha}$	112	0.17	128	0.07
	$^2J_{NC\alpha}$	111	0.24	128	0.08
	Total	351		384	
Flavodoxin	$^1J_{NC'}$	125	0.10	120	0.08
(aligned)	$^1J_{NC\alpha}$	112	0.20	117	0.17
	$^2J_{NC\alpha}$	111	0.28	117	0.16
	Total	348		354	

[a]Total numbers of coupling constants and pairwise RMSD values obtained from 3D quantitative *J*-correlated [^{1}H,^{15}N]-TROSY-HNC and control values obtained from spin-state selective 2D HN(α/β-NC′-*J*)-TROSY and HN(CO-α/β-NCα-*J*)-TROSY for the protein samples described in the text.

the average coupling magnitudes. As expected, the precision in the quantitative *J*-correlation experiment is mainly determined by sensitivity, because the uncertainty in the volume determination depends on the signal-to-noise ratio of the cross peaks.

Comparison with control experiments

Control $^1J_{NC'}$ couplings were determined from frequency differences in spin-state selective 2D HN(α/β-NC′-*J*)-TROSY, where the relevant doublet lines forming an E.COSY pattern are stored in separate subspectra after addition/subtraction of in-phase and antiphase spectra (Permi and Annila, 2000). Similarly, $^1J_{NC\alpha}$ and $^2J_{NC\alpha}$ values were simultaneously determined from 2D HN(CO-α/β-NCα-*J*)-TROSY spectra (Permi and Annila, 2000). Numbers of coupling constants and pairwise RMSD values calculated from repeated measurements are reported in Table 2. Quantitative *J*-correlated and spin-state selective experiments yielded similar numbers of coupling constants, the missing J_{NC} values being due to signal overlap rather than low signal intensities in both cases. Under the experimental conditions employed, measurement times were governed by resolution, leading to shorter periods for the two-dimensional control experiments compared to the three-dimensional quantitative *J*-correlation experiments. While reference peak intensities in 3D [^{15}N,^{1}H]-TROSY-HNC were higher than those of the corresponding signals in 2D HN(CO-α/β-NCα-*J*)-TROSY and of similar magnitude as those in 2D HN(α/β-NC′-*J*)-TROSY spectra, cross peak intensities were usually lower, affecting the precision of the quantitative *J*-correlation method. Consequently, RMSDs for the coupling constants obtained from the control experiments are lower compared to the quantitative *J*-correlation experiment. As for quantitative *J*-correlated [^{15}N,^{1}H]-TROSY-HNC, the reproducibility in the control experiments improves with increasing relative coupling magnitude from $^2J_{NC\alpha}$ to $^1J_{NC\alpha}$ to $^1J_{NC'}$, reflecting the ratio between the size of the splitting and the linewidth.

Nitrogen-carbon coupling constants obtained from two independent quantitative *J*-correlation measurements were averaged and compared to control values averaged from the spin-state selective experiments (Figure 4). Good agreement between results from both methods was achieved, with correlation coefficients $R^2 = 0.954$, $R^2 = 0.927$, and $R^2 = 0.925$ for $^1J_{NC'}$, $^1J_{NC\alpha}$, and $^2J_{NC\alpha}$, respectively. The regression equations for $^1J_{NC'}$, $^1J_{NC\alpha}$, and $^2J_{NC\alpha}$ are $y = 0.991$ x

+ 0.088, y = 0.872 x + 1.549, and y = 0.880 x + 0.956, respectively. A closer look at Figure 4B reveals that decreasing values of $^1J_{NC\alpha}$ tend to be larger from quantitative *J*-correlation than from HN(CO-α/β-NCα-*J*)-TROSY. In the latter, $^1J_{NC\alpha}$ couplings give rise to in-phase splittings in both subspectra corresponding to α and β spin states of C^α with respect to $^2J_{NC\alpha}$. It cannot be excluded that covariance effects between parameters from the ^1J coupling and the linewidth in F_1 result in slightly underestimated $^1J_{NC\alpha}$ coupling constants in the fitting procedure employed. Such an effect is absent when determining $^1J_{NC'}$ and $^2J_{NC\alpha}$ from spin-state selective spectra and, indeed, no systematic deviation between the two methods is observed (Figures 4A and 4C). After all, in the novel approach, all three types of coupling constants derive from a single quantitative *J*-correlation dataset with comparable intrinsic accuracy.

A source of error in α/β-filtered spin-state selective experiments is *J*-mismatch. When the actual *J*-coupling does not match the filter period τ, a dispersive signal component arises that usually has a small influence on scalar coupling values, but can be significant for RDCs. Usually, this is accounted for by a linear combination of in-phase and anti-phase spectrum components (Meissner et al., 1998; Permi and Annila, 2000; Permi et al., 2000). In coupling constants obtained by quantitative *J*-correlation, *J*-mismatch effects are absent and need not be corrected.

Dihedral-angle dependencies of J_{NC} *values*

The coupling constants $^1J_{NC\alpha(i)}$ and $^2J_{NC\alpha(i-1)}$ were found to depend on protein backbone conformation (Delaglio et al., 1991; Edison et al., 1994a, b; Wirmer and Schwalbe, 2002). The one-bond and two-bond $J_{NC\alpha}$ couplings obtained in the present work using the 3D quantitative *J*-correlated [^{15}N,^{1}H]-TROSY-HNC are plotted against ψ_i and ψ_{i-1} angles, respectively, from crystal structures of the three proteins (Figure 5). Correlations between $J_{NC\alpha}$ values and backbone ψ angles are clearly visible and in agreement with previously reported dihedral angle dependencies based on experimental data for ubiquitin, obtained with *J*-modulated HSQCs (Wirmer and Schwalbe, 2002) and for staphylococcal nuclease, obtained with ^{13}C-coupled [^{15}N,^{1}H]-HSQCs (Delaglio et al., 1991). The apparent large spread in the coupling data for like angles and deviations from the reported functions may be due to the fact that a one-dimensional *J*-ψ representation is not sufficient to represent the actual dihedral angle dependency of $J_{NC\alpha}$. In fact, it was already indicated that $^2J_{NC\alpha(i-1)}$ couplings seem to fit slightly better a more complex function depending on both ψ_{i-1} and ϕ_{i-1} angles (Edison et al., 1994a; Wirmer and Schwalbe, 2002). Amino-acid type dependencies as well as differences between torsion angles in crystal and solution structures cannot be excluded either as sources for the dispersion of *J* values for a given backbone conformation.

Protein nitrogen-carbon residual dipolar couplings

In addition to the measurements performed with isotropic flavodoxin, quantitative *J*-correlated [^{15}N, ^{1}H]-TROSY-HNC and spin-state selective control experiments were performed on a partially aligned flavodoxin system. Control ^{2}H-NMR experiments indicated variable quadrupolar splittings during different measurements, suggesting distinct alignment properties due to sample heating effects (data not shown). Moreover, during the total data acquisition period of approximately one week, the quadrupole splitting continuously decreased from 26 to 25 Hz. These observations corroborate the need for reliable experiments to obtain multiple couplings simultaneously.

The 3D quantitative *J*-correlated [^{15}N,^{1}H]-TROSY-HNC experiment, in addition to protein backbone ^{15}N-^{13}C dipolar couplings, can also yield tryptophan side chain $^1D_{N\varepsilon 1C\delta 1}$ and $^1D_{N\varepsilon 1C\varepsilon 2}$ couplings, as illustrated in Figure 3. In a similar manner, side chain ^{15}N-^{13}C dipolar couplings involving N^ε of arginines and $N^{\delta 1}$ or $N^{\varepsilon 2}$ of histidines are accessible, too, provided that the attached protons exchange sufficiently slowly with the solvent. Moreover, the protonated nitrogen N3 in the pyrimidine moiety of the flavinmononucleotide (FMN) isoalloxazine ring system is scalar coupled to two carbonyl carbons (C2 and C4) and one aromatic (C4a) carbon, allowing one to determine $^1D_{N3C4}$, $^1D_{N3C2}$, and $^2D_{N3C4a}$ dipolar couplings for the flavodoxin cofactor (Figure 3). In principle, these residual dipolar couplings form useful restraints for the orientations of side chain and cofactor with respect to the protein backbone.

Expected line broadening in the oriented state left aside, spectra recorded for the isotropic and oriented flavodoxin show peaks at virtually identical positions, critically indicating that the presence of the alignment medium does not alter the protein structure (Figure 3). Due to incomplete averaging of anisotropic shielding effects in the oriented protein, small chemical shift changes may be expected, especially for car-

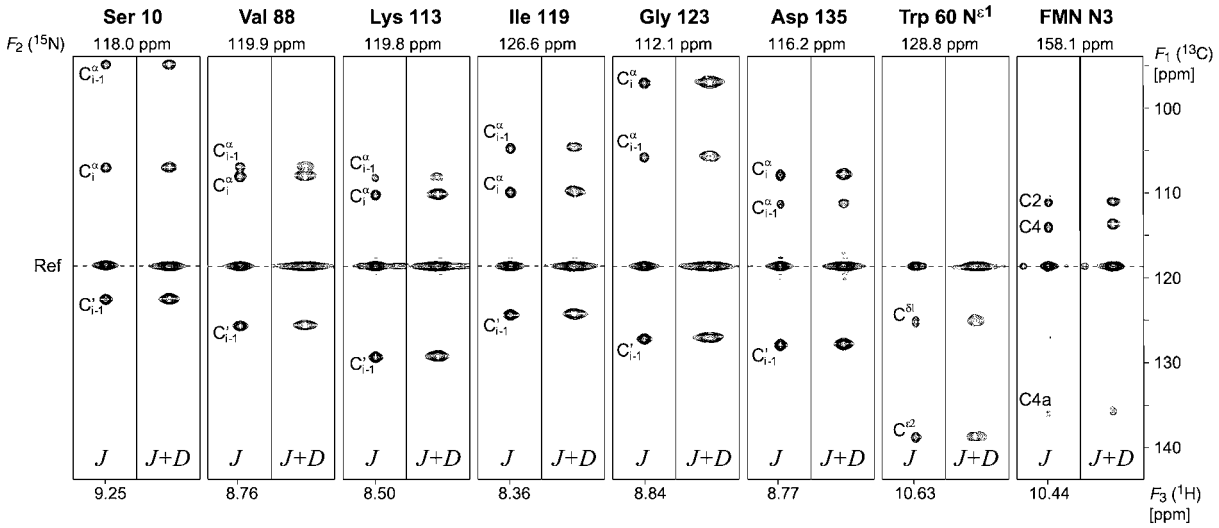

	Ser 10	Val 88	Lys 113	Ile 119	Gly 123	Asp 135				
$^1D_{NC'}$	1.96	-1.79	-0.74	-1.48	-1.06	-0.59	$^1D_{N\varepsilon 1C\delta 1}$	1.13	$^1D_{N3C4}$	-1.38
$^1D_{NC\alpha}$	-0.12	0.01	1.62	0.61	1.52	-0.01	$^1D_{N\varepsilon 1C\varepsilon 2}$	0.53	$^1D_{N3C2}$	0.29
$^2D_{NC\alpha}$	-0.07	-0.35	0.07	-0.25	0.02	-0.04			$^2D_{N3C4a}$	0.38

Figure 3. Selected $^1H^N$-^{13}C strips from 3D quantitative *J*-correlated [^{15}N,^1H]-TROSY-HNC spectra recorded for isotropic and aligned [^{15}N;^{13}C]-flavodoxin. Amino-acid assignments, ^{15}N frequencies and, for isotropic flavodoxin, also the $^1H^N$ frequencies are indicated. Dashed lines represent the ^{13}C carrier frequency. All cross peaks except for Trp60 $C^{\delta 1}$, $C^{\varepsilon 2}$ and FMN C4a are aliased once. Residual dipolar couplings, are given in Hz, as calculated from differences between averaged couplings obtained for the isotropic (*J*) and aligned (*J*+*D*) protein.

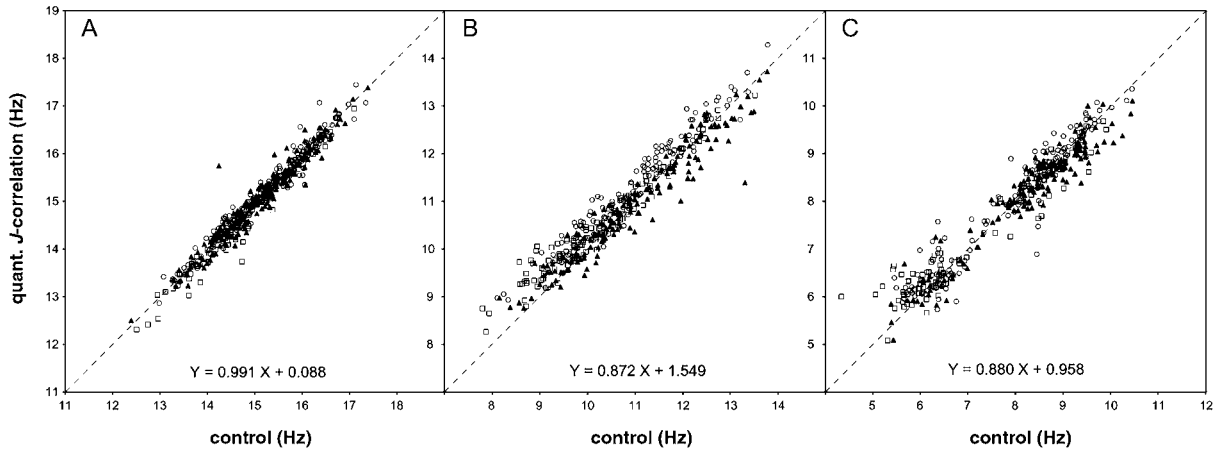

Figure 4. Correlation between nitrogen-carbon coupling constants obtained with 3D quantitative *J*-correlated [^{15}N,^1H]-TROSY-HNC experiments and control values using 2D HN(α/β-NC′-*J*)-TROSY and 2D HN(CO-α/β-NCα-*J*)-TROSY (Permi and Annila, 2000) for (A) $^1J_{NC'}$, (B) $^1J_{NC\alpha}$ and (C) $^2J_{NC\alpha}$. Most couplings are averages of repeated experiments. [^{15}N;^{13}C]-xylanase J_{NC} are depicted as filled triangles, [^2H;^{15}N;^{13}C]-DFPase J_{NC} as open circles and [^{15}N;^{13}C]-flavodoxin J_{NC} as open squares. Dashed lines present the diagonal of the figure; overall linear regression functions are indicated.

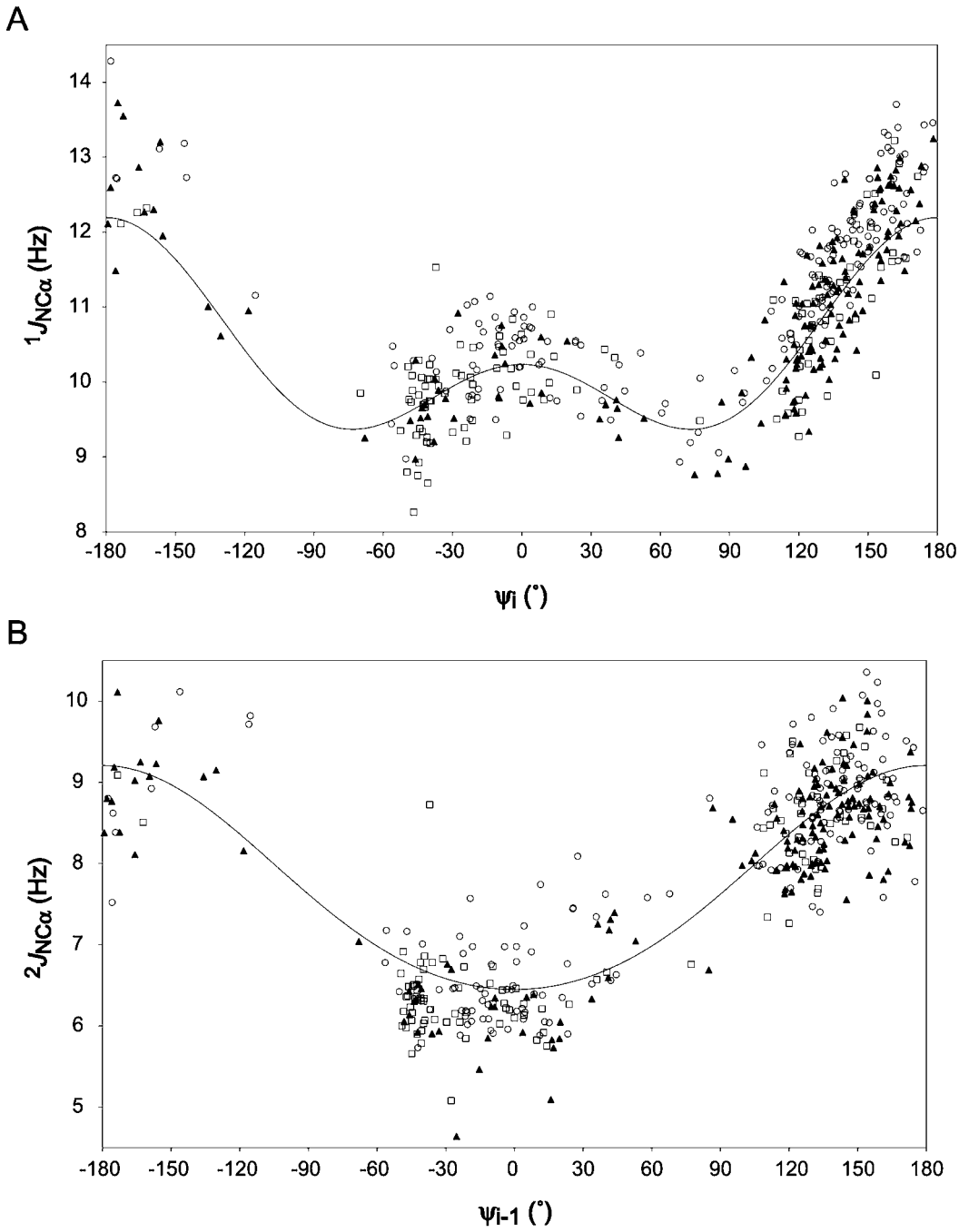

Figure 5. Protein backbone torsion-angle dependencies of couplings (A) $^1J_{NC\alpha(i)}$ on ψ_i and (B) $^2J_{NC\alpha(i-1)}$ on ψ_{i-1} for xylanase (filled triangles), DFPase (open circles) and flavodoxin (open squares). ψ-angles are obtained from X-ray datasets 1QH7 for xylanase (Sabini et al., 1999); 1E1A for DFPase (Scharff et al., 2001) and a refined version of 2FX2 for flavodoxin (Walsh, 1994; Walsh et al., 1998). Solid lines are torsion-angle dependencies as reported by Wirmer and Schwalbe (2002).

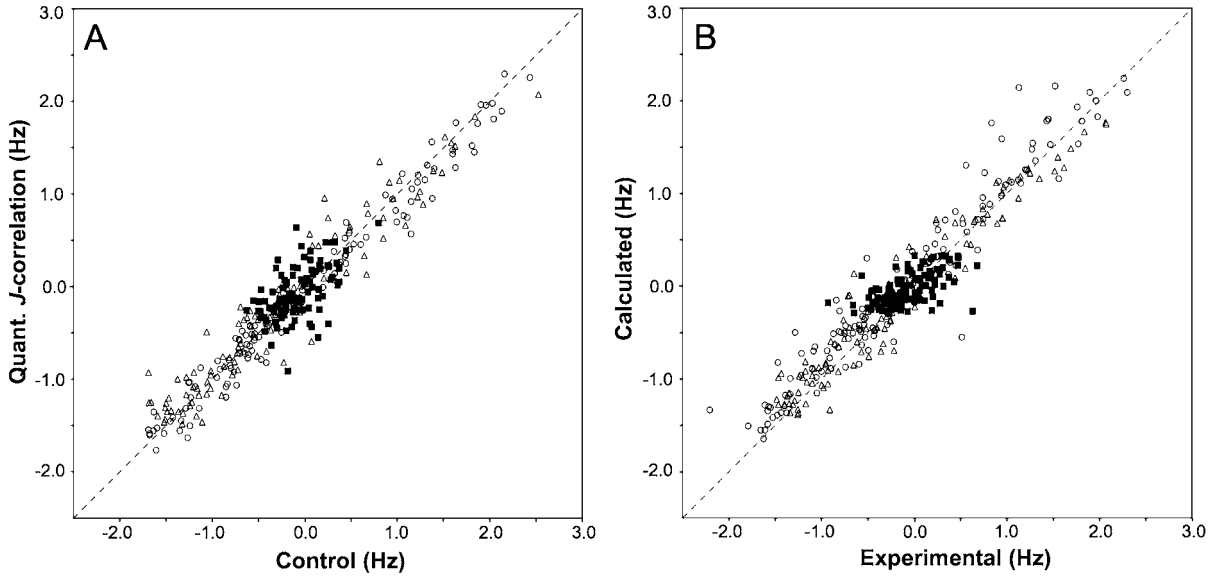

Figure 6. (A) Correlation between protein backbone ^{15}N-^{13}C residual dipolar couplings obtained from 3D quantitative *J*-correlated [^{15}N,^{1}H]-TROSY-HNC experiments and spin-state selective half-filter control experiments (Permi and Annila, 2000) for [^{15}N;^{13}C]-flavodoxin. (B) Comparison between the combined residual dipolar coupling values obtained with 3D quantitative *J*-correlated [^{15}N,^{1}H]-TROSY-HNC experiments and theoretical nitrogen-carbon RDCs back-calculated using the program PALES (Zweckstetter and Bax, 2000) on the flavodoxin X-ray structure 2FX2 (Walsh, 1994). $^{1}D_{\mathrm{NC'}}$ coupling constants are depicted as open circles, $^{1}D_{\mathrm{NC}\alpha}$ as open triangles and $^{2}D_{\mathrm{NC}\alpha}$ dipolar couplings as filled squares.

bonyl resonances (Cornilescu et al., 1998; Choy et al., 2001). However, such effects were not resolved in the present application due to coarse digitization of the ^{13}C dimension of [^{15}N,^{1}H]-TROSY-HNC spectra. Nitrogen-carbon $J + D$ values were determined for aligned flavodoxin. RDCs were calculated as differences between the coupling constants measured for the partially aligned ($J + D$) and isotropic (J) protein. Note that a comparison with control data becomes susceptible to errors in six different measurements, namely one quantitative *J*-correlation and two spin-state selective experiments for each isotropic and aligned flavodoxin. When considering the different types of RDCs separately, the correlation between the two methods decreases from $^{1}D_{\mathrm{NC'}}$ to $^{1}D_{\mathrm{NC}\alpha}$ to $^{2}D_{\mathrm{NC}\alpha}$ ($R^2 = 0.976$, 0.922, and 0.293, respectively). Clearly, $^{2}D_{\mathrm{NC}\alpha}$ coupling constants obtained from the quantitative *J*-correlation method are poorly correlated to those obtained from spin-state selective experiments because of low precision encountered in both approaches (Table 2). Due to the fact that the dipolar coupling scales with the relative distance between the two atoms considered, the precision of $^{2}D_{\mathrm{NC}\alpha}$ and the two-bond coupling itself are in the same order of magnitude. Therefore, the $^{2}D_{\mathrm{NC}\alpha}$ couplings obtained with quantitative *J*-correlation method as well as with spin-state selective method cannot be used to obtain protein structure information.

The program PALES (Zweckstetter and Bax, 2000) allows the calculation of the molecular alignment tensor by fitting a molecular coordinate set to a set of experimental RDCs, whereby theoretical RDC values are delivered for each experimental input value. RDCs obtained with the quantitative *J*-correlation method were checked against the crystal structure of oxidized flavodoxin (Walsh, 1994; Walsh et al., 1998). The individual sets of $^{1}D_{\mathrm{NC'}}$ and $^{1}D_{\mathrm{NC}\alpha}$ values show reasonable agreement between experimental and back-calculated dipolar couplings (Figure 6B; $R^2 \approx 0.93$ for $^{1}D_{\mathrm{NC}}$ and $^{1}D_{\mathrm{NC}\alpha}$). As anticipated, the correlation between the $^{2}D_{\mathrm{NC}\alpha}$ and the flavodoxin structure is poor ($R^2 \approx 0.31$).

Conclusions

A novel quantitative *J*-correlation experiment, 3D [^{15}N,^{1}H]-TROSY-HNC, was described which allows scalar and dipolar couplings to be determined between ^{15}N and ^{13}C in isotope-enriched biomolecules. Equally applicable to protonated and deuterated samples, the experimental set-up is simpler than for

alternative approaches based on spin-state selective filters. Intensity-encoding of the coupling constants, as opposed to concepts based on multiplet splittings, guarantees highest sensitivity with minimal peak overlap, thereby extending the size limit for the molecules that can be studied. Internal referencing of signal intensities obviates the need for recording a separate 2D reference spectrum. Various different N-C coupling types are simultaneously obtained, consequently lending the method robustness against variation in experimental conditions, especially those encountered in partial-alignment studies, and finally minimizing the number of experiments needed to record a complete structure dataset.

Additional material available

Two tables containing acquisition parameters for the spin-state selective 2D HN(α/β-NC′-*J*)-TROSY and 2D HN(CO-α/β-NCα-*J*)-TROSY control experiments are available on request.

Acknowledgements

We are grateful to Novo-Nordisk for providing the gene for the Family-11 xylanase plasmid and to Marco Betz for preparing the [^{15}N;^{13}C]-labeled xylanase sample. Judith Hartleib and Vicky Katsemi are thanked for providing [^{2}H;^{15}N;^{13}C]-labeled DFPase. Martin Walsh is thanked for the high-resolution X-ray coordinate set of flavodoxin. All spectra were recorded at the European Large Scale Facility for Biomolecular NMR at the university of Frankfurt. H.L.J.W. acknowledges a fellowship from the Alexander-von-Humboldt Foundation. M.M.M. would like to thank the Deutscher Akademischer Austauschdienst (DAAD) for a fellowship. This work was supported by a grant from the European Union (QLG2-CT-1999-01003).

References

Bax, A., Griffey, R.H. and Hawkins, B.L. (1983) *J. Magn. Reson.*, **55**, 301–315.

Bax, A., Kontaxis, G. and Tjandra, N. (2001) *Meth Enzymol.*, **339**, 127–174.

Bax, A., Vuister, G.W., Grzesiek, S., Delaglio, F., Wang, A.C., Tschudin, R. and Zhu, G. (1994) *Meth. Enzymol.*, **239**, 79–105.

Bendall, M.R., Pegg, D.T. and Doddrell, D.M. (1983) *J. Magn. Reson.*, **52**, 81–117.

Chou, J.J., Delaglio, F. and Bax, A. (2000) *J. Biomol. NMR*, **18**, 101–105.

Choy, W.-Y., Tollinger, M., Mueller, G.A. and Kay, L.E. (2001) *J. Biomol. NMR*, **21**, 31–40.

Cordier, F. and Grzesiek, S. (1999) *J. Am. Chem. Soc.*, **121**, 1601–1602.

Cornilescu, G., Marquardt, J.L., Ottiger, M. and Bax, A. (1998) *J. Am. Chem. Soc.*, **121**, 6836–6837.

Cornilescu, G., Ramirez, B.E., Frank, M.K., Clore, G.M., Gronenborn, A.M. and Bax, A. (1999*) J. Am. Chem. Soc.*, **121**, 6275–6279.

Curley, G.P., Carr, M.C., Mayhew, S.G. and Voordouw, G. (1991) *Eur. J. Biochem.*, **202**, 1091–1100.

Czisch, M. and Boelens, R. (1998) *J. Magn. Reson.*, **134**, 158–160.

De Alba, E. and Tjandra, N. (2002) *Prog. NMR Spectrosc.,* **40**, 175–197.

De Alba, E., Suzuki, M. and Tjandra, N. (2001) *J. Biomol. NMR*, **19**, 63–67.

Delaglio, F., Torchia, D.A. and Bax, A. (1991) *J. Biomol. NMR*, **1**, 439–446.

Dingley, A.J. and Grzesiek, S. (1998) *J. Am. Chem. Soc.*, **120**, 8293–8297.

Dosset, P., Hus, J.-C., Marion, D. and Blackledge, M. (2001) *J. Biomol. NMR*, **20**, 223–231.

Edison, A.S., Markley, J.L. and Weinhold, F. (1994a) *J. Biomol. NMR*, **4**, 519–542.

Edison, A.S., Weinhold, F., Westler, W.M. and Markley, J.L. (1994b) *J. Biomol. NMR*, **4**, 543–551.

Grzesiek, S. and Bax, A. (1993) *J. Am. Chem. Soc.*, **115**, 12593–12594.

Hartleib, J. and Rüterjans, H. (2001) *Protein Exp. Purif.*, **21**, 210–219.

Heikkinen, S., Permi, P. and Kilpeläinen, I. (2001) *J. Magn. Reson.*, **148**, 53–60.

Hu, J.-S. and Bax, A. (1997) *J. Biomol. NMR*, **9**, 323–328.

Juranić, N. and Macura, S. (2001) *J. Am. Chem. Soc.*, **123**, 4099–4100.

Juranić, N., Ilich, K.P. and Macura, S. (1995) *J. Am. Chem. Soc.*, **117**, 405–410.

Juranić, N., Likić, V.A., Prendergast, F.G. and Macura, S. (1996) *J. Am. Chem. Soc.*, **118**, 7859–7860.

Kay, L.E., Xu, G.Y. and Yamazaki, T. (1994) *J. Magn. Reson.*, **A109**, 129–133.

Knauf, M.A., Löhr, F., Curley, G.P., O'Farrell, P., Mayhew, S.G., Müller, F. and Rüterjans, H. (1993) *Eur. J. Biochem.*, **213**, 167–184.

Konrat, R., Muhandiram, D.R., Farrow, N.A. and Kay, L.E. (1997) *J. Biomol. NMR*, **9**, 409–422.

Kupče, Ē and Freeman, R. (1995) *J. Magn. Reson.*, **A115**, 273–276.

Kupče, Ē, Boyd, J. and Campbell, I.D. (1995) *J. Magn. Reson.*, **B106**, 300–303.

Löhr, F. and Rüterjans, H. (2000) *J. Magn. Reson.*, **146**, 126–131.

Löhr, F., Mayhew, S.G. and Rüterjans, H. (2000) *J. Am. Chem. Soc.,* **122**, 9289–9295.

Löhr, F., Pérez, C., Schmidt, J.M. and Rüterjans, H. (1999) *Bull. Magn. Reson.,* **20**, 9–14.

Loria, J.P., Rance, M. and Palmer III, A.G. (1999) *J. Magn. Reson.*, **141**, 180–184.

Matsuo, H., Kupče, Ē., Li, H. and Wagner, G. (1996) *J. Magn. Reson.*, **B111**, 194–198.

Meissner, A., Schulte-Herbrüggen, T. and Sørensen, O.W. (1998) *J. Am. Chem. Soc.*, **120**, 7989–7990.

Ottiger, M., Delaglio, F. and Bax, A. (1998) *J. Magn. Reson.*, **131**, 373–378.

Permi, P. and Annila, A. (2000) *J. Biomol. NMR*, **16**, 221–227.
Permi, P., Rosevear, P.R. and Annila, A. (2000) *J. Biomol. NMR*, **17**, 43–54.
Pervushin, K., Riek, R., Wider, G. and Wüthrich, K. (1997) *Proc. Natl. Acad. Sci. USA*, **94**, 12366–12371.
Pervushin, K.V., Wider, G. and Wüthrich, K. (1998) *J. Biomol. NMR*, **12**, 345–348.
Rückert, M. and Otting, G. (2000) *J. Am. Chem. Soc.*, **122**, 7793–7797.
Sabini, E., Sulzenbacher, G., Dauter, M., Dauter, Z., Jørgensen, P.L., Schülein, M., Dupont, C., Davies, G.J. and Wilson, K.S. (1999) *Chem. Biol.*, **6**, 483–492.
Salzmann, M., Pervushin, K., Wider, G., Senn, H. and Wüthrich, K. (1998) *Proc. Natl. Acad. Sci. USA*, **95**, 13585–13590.
Scharff, E.I., Koepke, J., Fritzsch, G., Lücke, C. and Rüterjans, H. (2001) *Structure*, **9**, 493–502.
States, D.J., Haberkorn, R.A. and Ruben, D.J. (1982) *J. Magn. Reson.*, **48**, 286–292.
Stonehouse, J., Shaw, G.L., Keeler, J. and Laue, E.D. (1994) *J. Magn. Reson.*, **A107**, 178–184.
Tjandra, N. and Bax, A. (1997) *J. Am. Chem. Soc.*, **119**, 9576–9577.
Tycko, R., Pines, A. and Guckenheimer, R. (1985) *J. Chem. Phys.*, **83**, 2775–2802.
Vuister, G.W. and Bax, A. (1993a) *J. Am. Chem. Soc.*, **115**, 7772–7777.
Vuister, G.W. and Bax, A. (1993b) *J. Magn. Reson.*, **B102**, 228–231.
Vuister, G.W., Yamazaki, T., Torchia, D.A. and Bax, A. (1993) *J. Biomol. NMR*, **3**, 297–306.
Walsh, M.A. (1994) Ph.D. Thesis, National University of Ireland.
Walsh, M.A., McCarthy, A., O'Farrell, P.A., McArdle, P., Cuningham, P.D., Mayhew, S.G. and Higgins, T.M. (1998) *Eur. J. Biochem.*, **258**, 362–371.
Wang, Y.-X., Jacob, J., Cordier, F., Wingfield, P., Stahl, S.J., Lee-Huang, S., Torchia, D., Grzesiek, S. and Bax, A. (1999) *J. Biomol. NMR*, **14**, 181–184.
Weigelt, J. (1998) *J. Am. Chem. Soc.*, **120**, 10778–10779.
Wirmer, J. and Schwalbe, H. (2002) *J. Biomol. NMR*, **23**, 47–55.
Zweckstetter, M. and Bax, A. (2000) *J. Am. Chem. Soc.*, **122**, 3791–3792.